Hindawi
Advances in Materials Science and Engineering
Volume 2020, Article ID 5708969, 16 pages
https://doi.org/10.1155/2020/5708969

*Research Article*

# Tensile Fracture Behavior of Corroded Pipelines: Part 2—Numerical Simulation Based on Monte Carlo Method

**Feng Liu**,[1] **Yuchao Yang**,[1] **and Feng Xi**[2]

[1]*Shandong University of Science and Technology, Shandong Provincial Key Laboratory of Civil Engineering Disaster Prevention and Mitigation, Qingdao 266590, China*
[2]*School of Civil Engineering, Shandong Jianzhu University, Jinan 250101, China*

Correspondence should be addressed to Feng Liu; feng.liu@sdust.edu.cn

Received 15 September 2019; Revised 14 February 2020; Accepted 17 February 2020; Published 4 April 2020

Academic Editor: Tetsu Yonezawa



The experimental part in this companion paper revealed that the macroscopic mechanical performance of corroded pipes follows a decreasing trend with the increasing corrosion rate. Inspired by the surface topology by scanning electronic microscopy (SEM) and the scattered distribution of test data, a computational procedure based on the Monte Carlo simulation method was developed in this paper to understand the randomness of the crack propagation process and the performance degradation mechanism of the corroded pipelines. A total of 2700 random samples, which contain three corrosion rates of 15%, 45%, and 70% with each corrosion rate having three variances of 0.02 mm, 0.06 mm, and 0.10 mm, were generated and then were mapped to the shell section of the FE model. In the application of the material model considering the damage, a series of "numerical" tensile experiments were carried out. The simulation analysis indicated that the corrosion rate and the standard variance of the thickness collaboratively dominated the mechanical performance of the corroded specimen. Under the same standard deviation, the wall corresponding to the higher corrosion rate is more likely to cause stress concentration in the weak position, which makes the pipe more prone to fail. Furthermore, under the same corrosion rate, the increase of the standard deviation will aggravate the unevenness of the wall thickness distribution, and then the lower tensile load will cause damage at weak locations and lead to randomness of the crack propagation path, thereby reducing the pipe's macroscopic strength and fracture strain. The analytical methods in this paper have the potential of being a useful tool for structural reliability assessments of aged pipelines and the full life cycle design of new pipeline networks.

## 1. Introduction

Owing to its large transportation volume, continuity, and economic efficiency, metal pipelines have become the artery of modern industrial fluid transport. However, due to the working conditions and aging, these pipelines are extremely vulnerable to external environmental erosion, which causes defects in the components and reduces its reliability. Research studies by Ossai [1], Fekete and Varga [2], and Pilkey et al. [3] showed that corrosion is becoming a severe threat to the safety of pipelines.

Extensive research on the performance of corroded pipelines focuses on the burst pressure [4–9] and bending capacity [10–16], and there are few studies on their tensile behavior. In the experimental part of this companion paper [17], a total of 210 pipes were corroded from grade 10% to 70%, and the tensile test was carried out according to the standard experimental method. The observation based on the fracture patterns of corroded pipelines shows that the corrosion transits the fracture mode from the transverse crack in the middle of the specimen to a multiple fracture mode in which the position and angle are randomly distributed. These transitions significantly affect the macroscopic mechanical properties such as yield strength and tensile strength of the pipeline, and the magnitude of this influence increases sharply with the increase of the corrosion rate. However, due to the limitations of experimental conditions and observational measurement techniques, the experimental results and conclusions obtained would be not comprehensive and objective. Detailed numerical

simulation is needed to gain more accurate understanding of the pipe's stretching behavior. This need motivates the present study.

Presently, there are two main challenges in the application of numerical means to study the mechanical behavior of corroded pipes. One is the characterization and simulation of the corrosion characteristics of the pipe's surface. Some scholars believe that the degree of reduction in section thickness caused by corrosion is a critical factor in determining the behavior of the pipeline. Therefore, the rust of a specific shape such as a semielliptical, parabolic, rectangular, or conical shape with varying depth is used to construct the numerical model [18–22]. This method calculates the geometry of the corroded area based on a simple geometric formula without fully considering the randomness of the wall thickness distribution. This is significantly different from the real characteristics caused by the intrusion of pipes in a complex natural environment. And, the second difficulty is reflected in how numerical calculations accurately consider the damage behavior of materials and how to statistically analyze the discreteness of calculation results caused by the random distribution of wall thickness.

This paper develops a simulation method based on Monte Carlo simulation (MCS). Based on the stochastic theory, the wall thickness field which has three kinds of corrosion rates including 15%, 45%, and 70% with each of the corrosion rate having three standard deviations of 0.02 mm, 0.06 mm, and 0.10 mm, was generated. And a corresponding number of FE analyses were carried out. Based on the comparison of the fracture mode and macroscopic strength evolution, the mechanism of the corrosion degrades the macroscopic mechanical behavior of the pipeline was studied.

The outline of the paper is as follows: in the next section, FE modelling and construction of a random thickness distribution that matches the surface topology of the corroded specimen are described. The analysis of typical numerical results is presented in Section 3 to discuss the fracture mechanism of corroded pipes. The MCS results are discussed in Section 4 to demonstrate the importance of corrosion rate and standard variance, which is followed by conclusions.

## 2. FE Model and Analysis Method

*2.1. Modelling Procedure.* In the present study, the general FE analysis package, ABAQUS [23], was used to conduct the simulation. Inspired by the scattered distribution of test data and SEM photographs of the corroded surface topology, the following simulation strategy was designed to investigate the thickness heterogeneity induced from the corrosion on the performance degradation and fracture behavior of the pipeline:

(i) The pipeline was constructed and meshed using ABAQUS/CAE, and an input file was generated that included the node and element information. Since the fracture path is always dependent upon the initial mesh, a triangular element type S3 was adopted for the entire model to ensure that the curved crack could be modelled with high accuracy.

(ii) A series of random fields were generated that included the thickness of the specimen according to the original dimension of pipe, grid point, and the control parameters related to the corrosion rate and the standard deviation. It should be noted that material properties, such as elastic modulus, Poisson's ratio, and strength, may decrease due to the process of the corrosion, but these were not the focus of the present study and were not considered.

(iii) The distribution of thickness generated in (ii) was mapped to the FE model to complete the shell section definition. As discussed in the test section presented in Part 1 of this companion paper [17], this study only aimed to understand the mechanical behavior of the outside surface corroded specimen, so the shell section offset technique was activated to ensure all inside surfaces of the pipe were in the same circumstance plane.

(iv) An analysis was performed using the ABAQUS solver considering the material degrading.

(v) Steps (ii)–(iv) were repeated for a sufficient number of random samples as required by the MCS method, and then statistical analysis was performed.

*2.2. Mechanical Model and Loading Strategy.* Figure 1 Illustrates the mechanical model of a corroded pipe whose geometry dimension and boundary conditions are strictly consistent with the description in the experiment part [17]. The model was subjected to uniformly distributed axial displacement at the right side of the specimen. To investigate the mesh dependence, the following models were used to conduct the mesh sensitivity analysis: the coarse mesh had 2,349 nodes and 4,356 shell elements, the intermediate mesh had 8,374 nodes and 16,256 shell elements, and the fine mesh had 32,424 nodes and 64,256 shell elements.

In addition, since the implicit solver may encounter convergence difficulties after initiation of damage, the ABAQUS/Explicit module was used to conduct the present analysis. To ensure the accuracy of the results, sufficient loading time was required in simulation analysis to eliminate the influence of the inertia effect. A loading period of 0.1 second for the model with intermediate mesh and $l_c$ of 1.5 mm (discussed in Section 2.3) was finally selected for the following simulation analysis after a comparison of the time histories of the reaction force obtained from the batch of results for the periods of 0.01 s, 0.03 s, 0.05 s, and 0.1 s for three models.

*2.3. Corroded Surface Characterized as a Random Field.* The scanning electron micrographs and experimental results of the corroded pipelines indicated that the thickness of the tube wall is nonuniform due to environmental erosion, which can be described by a random distribution field.

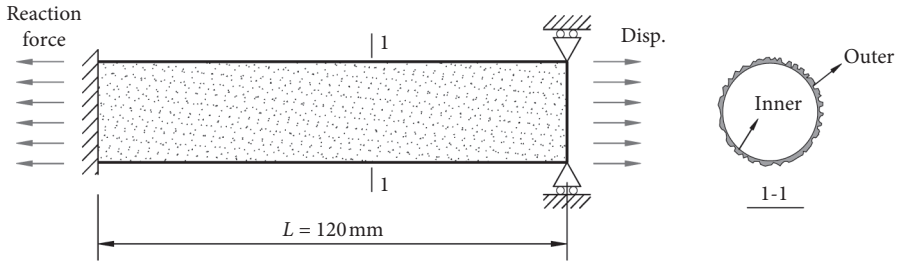


Figure 1: Pipe specimen under uniaxial stretch loading.

Without loss of generality, the thickness $T$ can be described by

$$T = T(x, \omega), \tag{1}$$

where $x$ and $\omega$ are the pipe size vector and random field, respectively.

The spectral decomposition described in [24] was used to generate a stationary Gaussian random field, $T(x, \omega)$, with zero mean and unit variance. In this process, the correlation function $\rho(x_1, x_2)$ was chosen as

$$\rho(x_1, x_2) = \exp\left[-\frac{|x_1 - x_2|^2}{{l_c}^2}\right], \tag{2}$$

where $x_1$ and $x_2$ represent the coordinate position of the tube wall in the longitudinal and circumferential directions. And $l_c$ is the characteristic length whose value is closely related to the degree of corrosion. Three sets of constant values of $l_c$, i.e., 3 mm, 1.5 mm, and 0.75 mm, were set to generate the random thickness field. They are within the range of corroded pit sizes that normally existed in the pipeline.

Considering the wall thickness does not strictly follow a stationary random distribution, equation (1) is transformed to a nonstationary distribution using equation (3) [25]:

$$T(x, \omega) = T_0 + F^{-1}(\Phi(X(x, \omega))), \tag{3}$$

where $\Phi(\cdot)$ is the standard normal cumulative density function, $F(\cdot)$ is the marginal cumulative probability density function, and $T_0$ is the mean value of thickness. The readers are suggested to refer to paper [25] for more detailed description.

A MATLAB [26] script was written based on the above procedure to generate the random distribution of the element thickness. Figure 2 presents a typical field of wall thickness for a pipe that has an average thickness of 0.85 mm and standard variance of 0.06 mm. Then, the random field can be mapped to the shell section of the FE model. Figure 3 shows a typical FE model with intact and corroded walls with the shell thickness shown in Figure 2. It can be seen that the thickness of each element of the intact pipeline model is uniform in both the inside and outside surfaces compared to the corroded one with a "rugged" outside and smooth inside surface. Furthermore, Figures 4 and 5 show a plurality of sets of pipe sections along the axial and vertical axes. These arrangements are consistent with the observations from the SEM photographs as described in Part 1 of this companion paper [17].

In addition, since the original pipeline wall thickness used in this experiment and simulation was 1 mm, the "perforation" and "overflow" phenomenon of the pipe needed to be avoided during the assignment step. In this simulation, a value bigger than 1 mm was set to 1 mm and a value less than or equal to 0 had a value of $10^{-3}$ mm.

*2.4. Modelling of Tensile Failure in ABAQUS Environment.* As shown in Figure 6, the progressive damage model provided by ABAQUS [23] was used in the present model to detect and trace damage initiation and evolution in the material at integration points in the element until complete failure. The model used the equivalent plastic strain at the onset of damage, $\bar{\varepsilon}_0^{pl}$, as the failure initiation criterion. Research by Mirza et al. [27] and Wierzbicki et al. [28] indicated that the value of rupture strain is sensitive to the strain rate and stress triaxiality, and there does not exist a formula to be used to define it. However, for the pipe studied in the present paper, the hoop stress is small since the pipe only subjected to uniaxial tension, and the stress state of the pipe is approximately considered as a uniaxial stress state. In this paper, the plastic fracture strain measured by the tensile test for original steel pipe material (see Figure 7) is selected as $\bar{\varepsilon}_0^{pl}$, and the corresponding stress triaxiality is 0.33.

Material degradation starts when the damage initiation criterion is met based on the following condition:

$$\Phi_f = \frac{\sum \Delta\varepsilon^{pl}}{\bar{\varepsilon}_0^{pl}} = 1, \tag{4}$$

where $\sum \Delta\varepsilon^{pl}$ is an accumulative value of the equivalent plastic strain at the integration points.

Once damage initiation has been detected, the damage process continues, and the damage evolution can be traced assuming a linear relationship of the damage variable with the effective plastic displacement [23]. The damage variable represents the accumulated ratio of the effective plastic displacement, $u^{pl}$, at integration points to the total plastic displacement at the point of failure $u_f^{pl}$, expressed as

$$u_f^{pl} = L_e\left(\bar{\varepsilon}_f^{pl} - \bar{\varepsilon}_0^{pl}\right), \tag{5}$$

where $L_e$ is the characteristic length of the element defined in the current model along the axial direction of the pipe. $\bar{\varepsilon}_f^{pl}$ is the equivalent plastic strain at complete failure of the material taken from the uniaxial stress-strain curve. During

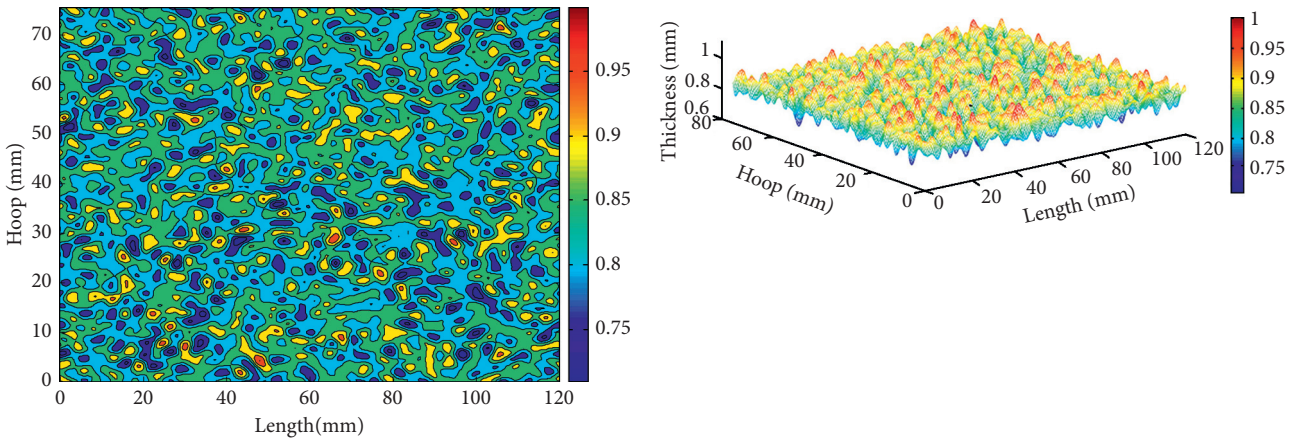


Figure 2: Generated random field of wall thickness along with the axial and hoop directions of a pipe with $\eta$ = 15% and var = 0.06 mm. (a) 2D. (b) 3D.

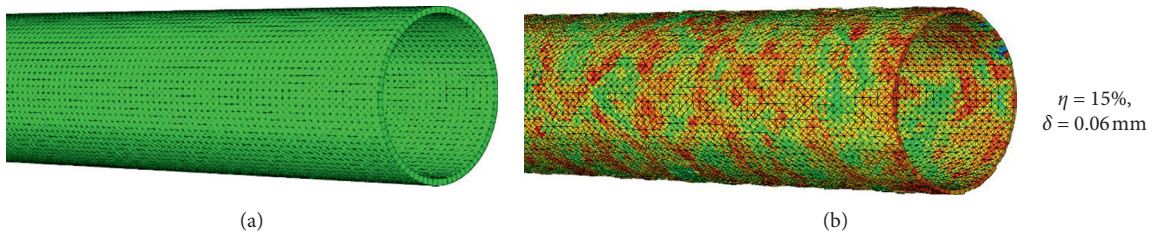


Figure 3: Comparison of surface topologies of an intact and corroded pipe in FE model. (a) Uncorroded. (b) Corroded.

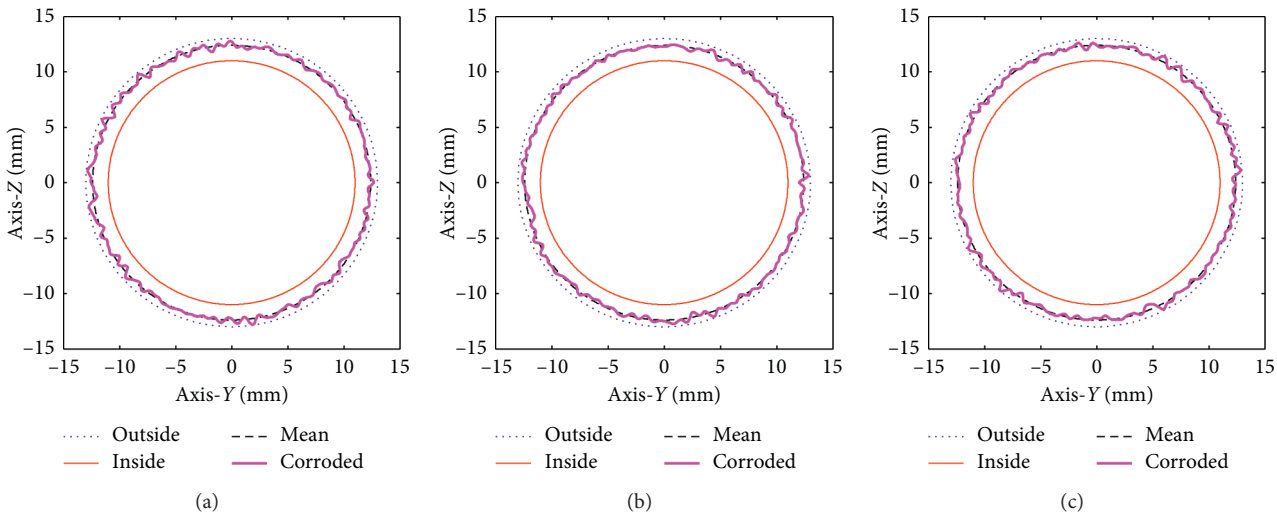


Figure 4: Continued.

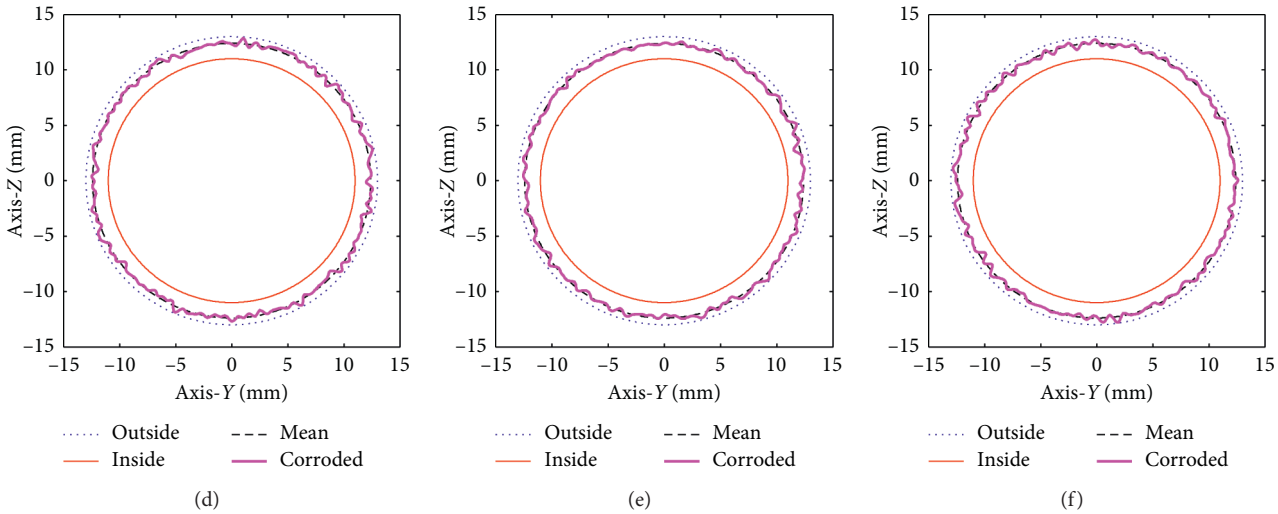


FIGURE 4: The topology of corroded section along the axis of pipe. (a) $X = 0$. (b) $X = L/5$. (c) $X = 2L/5$. (d) $X = 3L/5$. (e) $X = 4L/5$. (f) $X = L$.

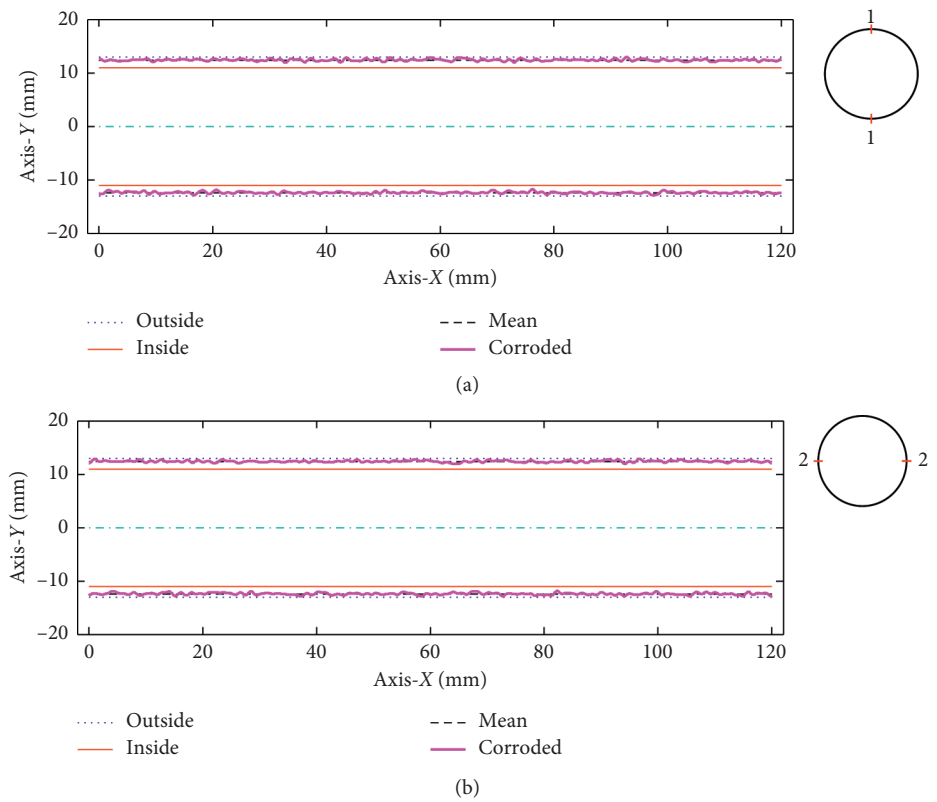


FIGURE 5: The topology of corroded section along the axis of pipe. (a) Section 1-1. (b) Section 2-2.

damage evolution, the stress of the material at each integration point can be expressed as

$$\sigma = (1 - D)\overline{\sigma}, \tag{6}$$

where $D$ is the degradation parameter, and its value ranges from 0 to 1, where 0 represents the onset of damage and 1 represents complete failure. When the element fails completely ($D = 1$), the failed element was removed from the model.

Table 1 shows the relevant parameters of the material used in the simulation. It should be emphasized that the stresses and strains listed in Table 1 are derived from the actual tensile stress and strain obtained by the standard tensile test of the pipe sheet directly. Due to the structural effect and the shrinkage effect of the failure surface, these parameters are quite different from the data directly measured from the pipe.

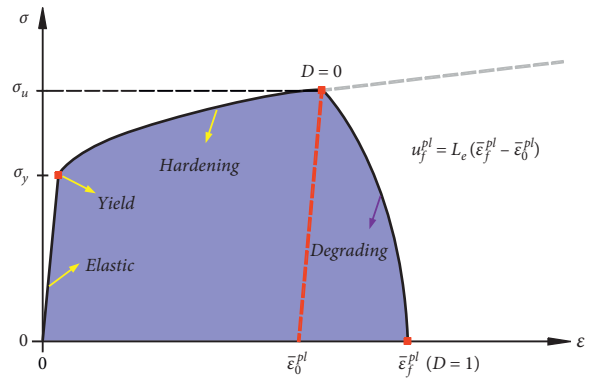


Figure 6: Progressive damage degradation model in ABAQUS [23].

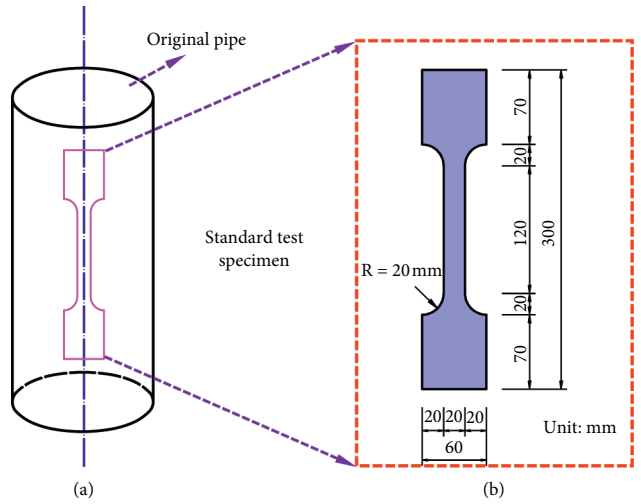


Figure 7: Standard tensile test for the material of pipe. (a) Original pipe. (b) Standard test specimen.

Table 1: Material failure parameters used in present numerical model.

| $\rho$ (kg/m$^3$) | $E$ ($GPa$) | $\nu$ | $\sigma_y$ (MPa) | $\sigma_u$ (MPa) | $\bar{\varepsilon}_0^{pl}$ | $\bar{\varepsilon}_f^{pl}$ | $u_f^{pl}$ (m) | Stress triaxiality |
|---|---|---|---|---|---|---|---|---|
| 7800 | 200 | 0.3 | 304 | 554 | 0.24 | 0.44 | 0.0004 | 0.33 |

## 3. Analysis of the Results of a Numerical Example

*3.1. Tensile Fracture in an Intact Pipe.* To verify the feasibility of the model and analysis method, a numerical simulation of an intact specimen was performed. The thickness of all shell sections in the FE model was defined as 1 mm. Figure 8 shows a comparison of the simulated stress-strain curve with that from a test of an intact specimen. It can be seen that the two curves agree well with each other both in stiffness and strength. Therefore, this result confirms the validity of the present simulation.

The sequence of the fracture pattern is illustrated in Figures 9(a)–9(c). It was found that the damage variable, $D$, increased along with an increase in the axial strain, but the position of the fracture was located in the middle of the model, and its shape was neat. A comparison of the failure model shown in Figure 9(c) with the real test specimen (see Figure 9(d)) shows it is consistent with the neat fracture of the intact pipeline. This indicates that the force was uniformly concentrated in the middle section.

The above comparison of stress-strain relationship and fracture behavior confirms that the numerical models and methods used in this paper are feasible. This method was applied to subsequent analysis for the corroded pipes.

*3.2. Significance for Modelling Thickness Heterogeneity.* To investigate the influence of pipe wall corrosion on its tensile behavior, Figure 10 shows a stress-strain curve and crack development process of a corroded pipe under uniaxial

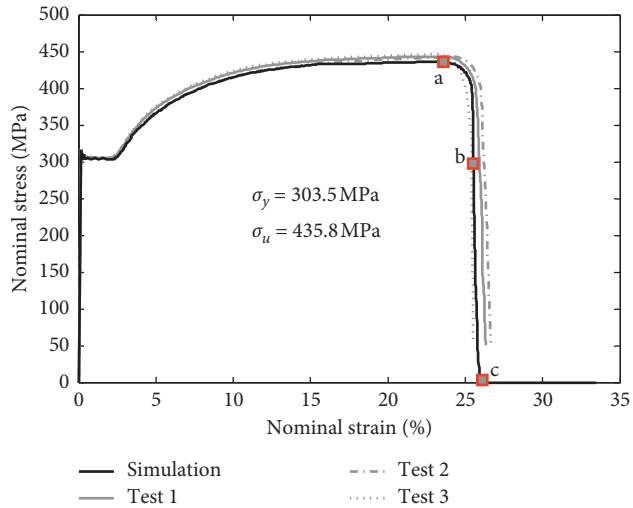


Figure 8: A comparison of simulated and recorded stress-strain curves.

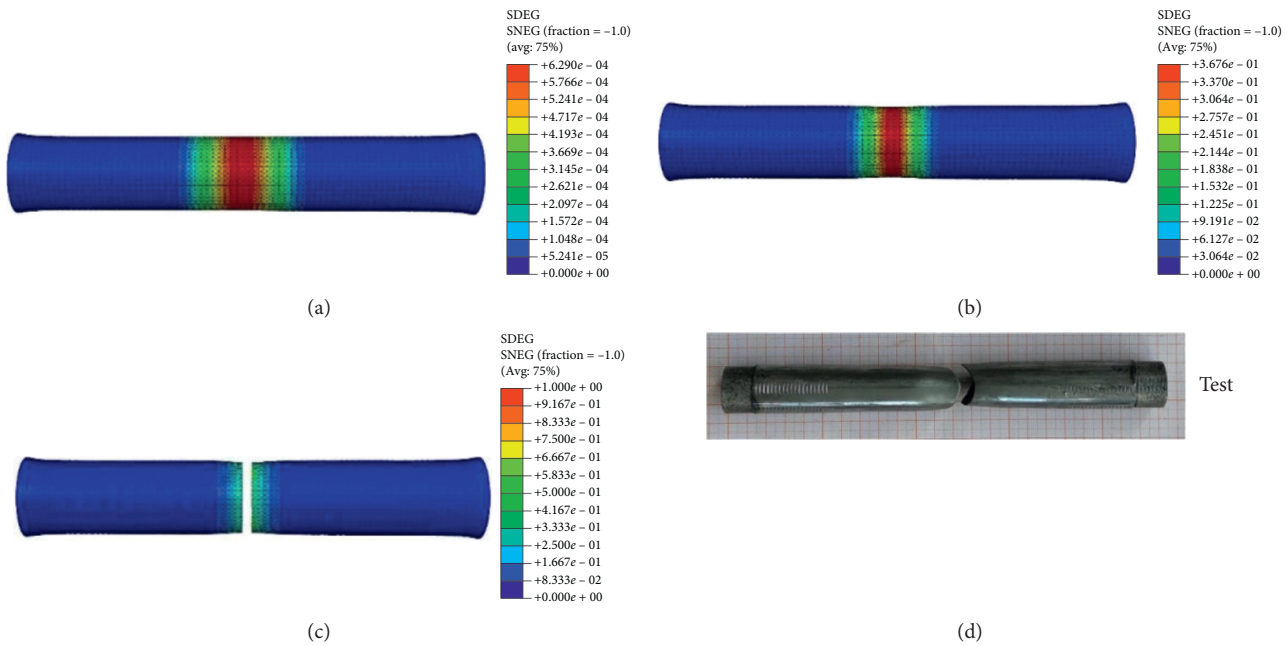


Figure 9: Evolution of fracture and failure mode of an intact pipe.

tension. The thickness field of the pipe is shown in Figure 10(a), which has a corrosion rate of $\eta = 70\%$ and standard deviation of $\delta = 0.10$ mm. Figure 10(b) shows the stress-strain relationship between the corroded and uncorroded pipe. It was found that the yield strength and tensile strength of the model are markedly reduced to 232.7 MPa and 373.4 MPa, respectively, and the strain corresponding to the peak stress was significantly reduced to 0.076, these suggesting that the corrosion of the section remarkably affects the pipe's plastic properties.

The fracture instants marked in Figure 10(b) are plotted in Figure 10(c). These figures indicate a remarkable difference from the results shown in Figure 9. For the corroded pipe shown in Figure 10, the initial fracture does not occur uniformly in the middle of the specimen, but on its right part in a scattered manner. As the fracture progressed, more adjacent cracks appeared, until two main paths were generated. These phenomena are consistent with the observation in the test (see Figure 10(c)).

As the service time increases, the pipe is inevitably nonuniform in thickness due to corrosion which is frequently controlled by various factors such as the external environment and materials properties. When subjected to stretching, the stress concentration tended to occur at the weaker part, which in turn leads to new stress concentrations in the adjacent pipe wall and successive failures. Such

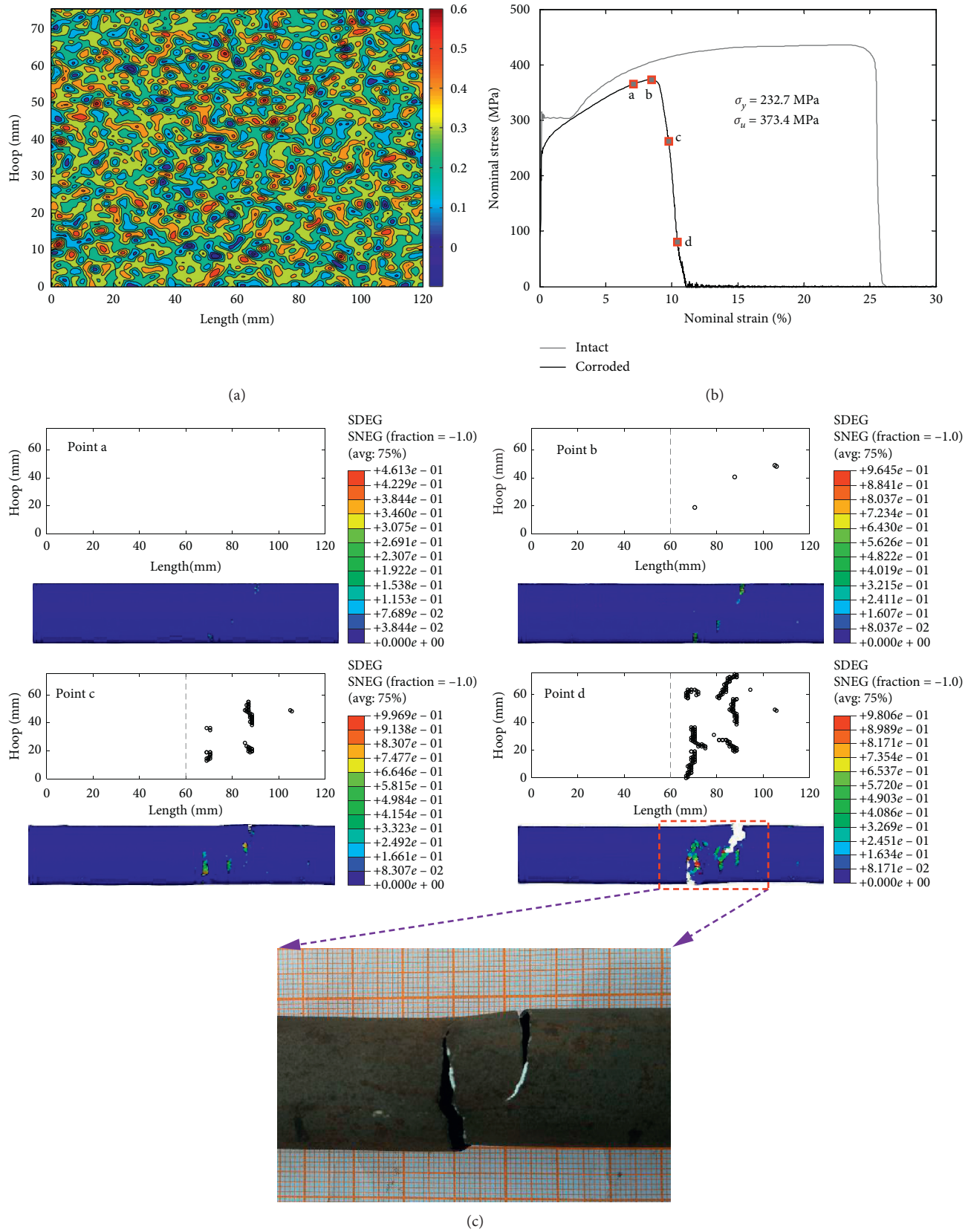


Figure 10: Damage evolution and fracture mode of a corroded pipe. (a) Random field with a value of $\eta$ = 70% and $\delta$ = 0.10 mm, (b) stress-strain curve, (c) crack propagation at points marked in (b) and crack observed in test specimen with $\eta$ = 71.02%.

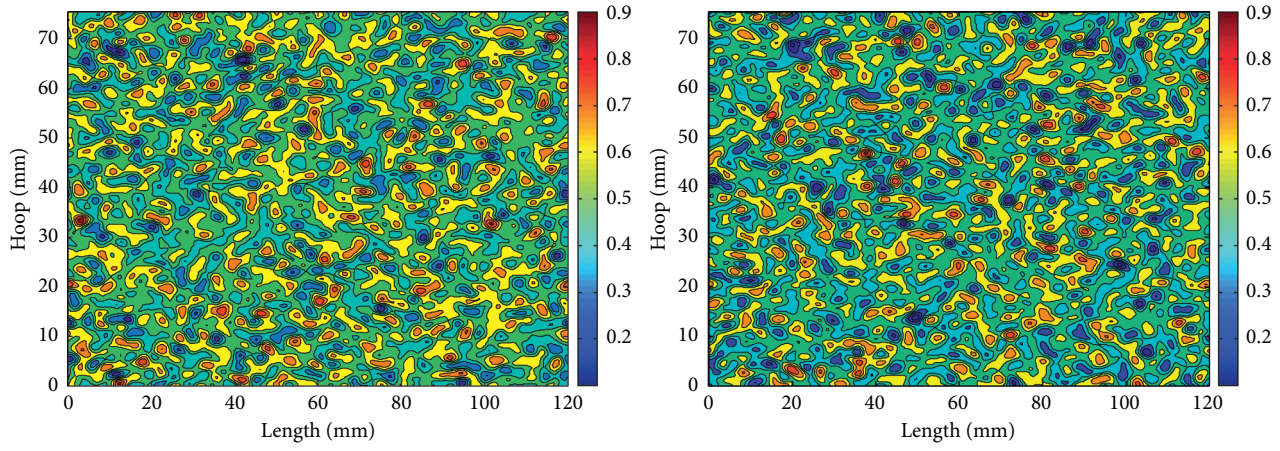


(a)

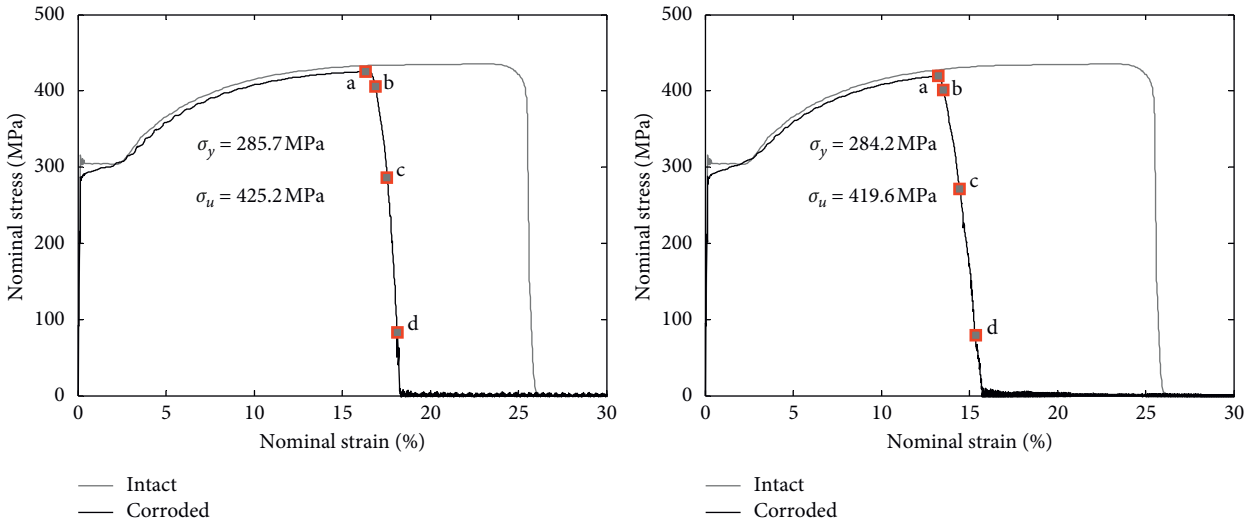


(b)

Figure 11: Continued.

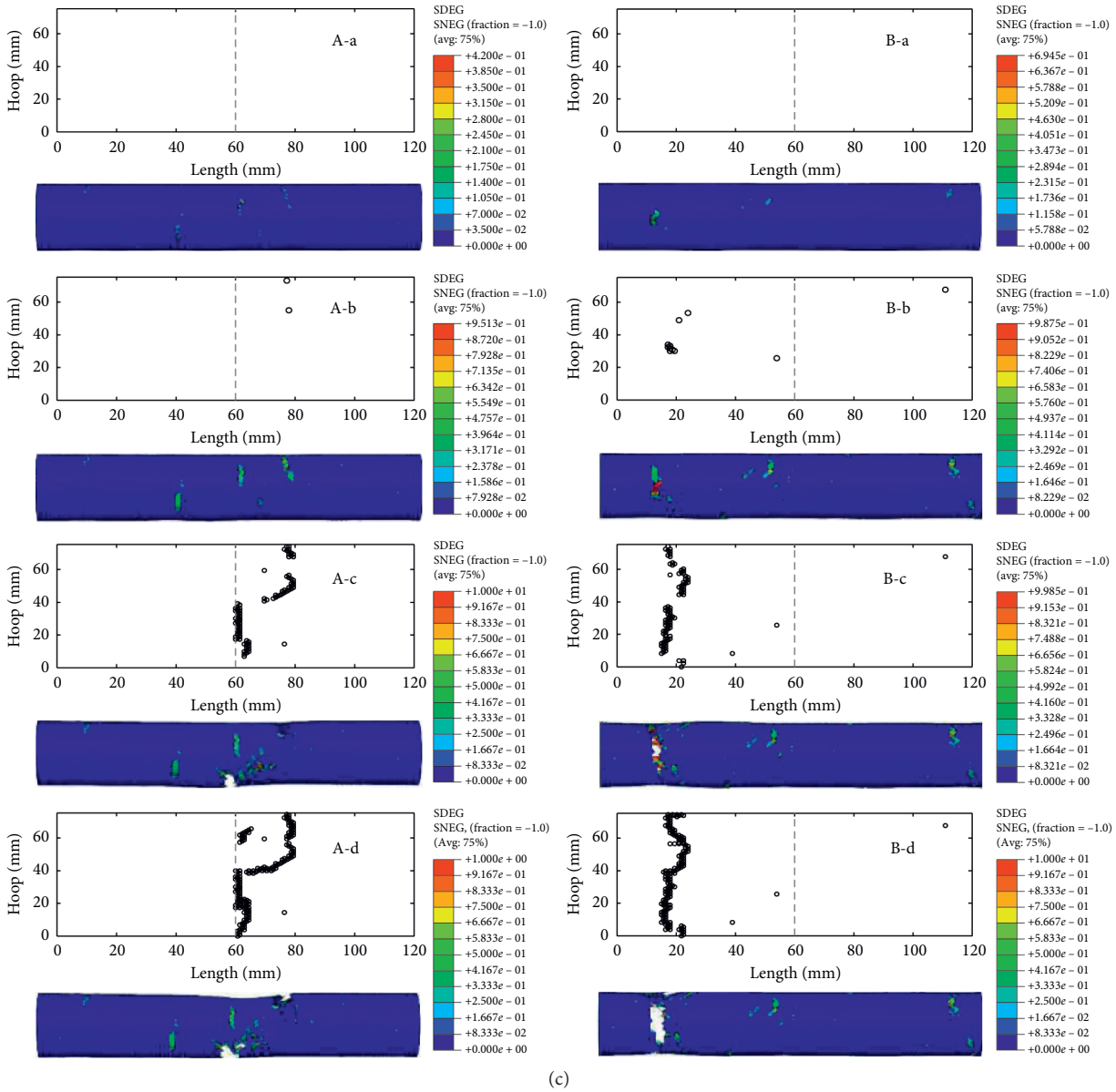


Figure 11: Damage evolution and fracture mode of corroded pipes with the same corrosion rate and variance. (a) Random field with a value of $\eta$ = 45% and var = 0.10 mm, (b) simulated stress-strain curve, and (c) crack propagation at the points marked in (b).

reciprocation causes an overall progressive fracture at the weak section of the entire tube wall. Then, it is reflected macroscopically as a decrease in strength and plasticity. These observations indicate that proper consideration of the heterogeneity of the wall thickness distribution of the model is critical to the accuracy of the prediction results when simulating the macroscopic mechanical properties of the corroded pipeline.

*3.3. Influence of Randomness on the Distribution Field.* To study the effect of the randomness of the thickness distribution on the surface field, two random distribution fields were generated using the same corrosion rate of $\eta$ = 45% and variance of $\delta$ = 0.1 mm, and then the simulation was conducted. The random field, reconstituted stress-strain curve, and the fracture process are shown in Figure 11. The yield stress and ultimate strengths are 285.7 MPa and 425.2 MPa, respectively, for the specimen with a left random distribution field, compared to 284.2 MPa and 419.6 MPa for the right one. For the specimen on the left column, the crack generated and evolved in the middle and right section of the specimen, compared to the left part for the right specimen.

It can be easily concluded that although the random field had the same parameters and obeyed the same generation principal, it did not yield the same strength and fracture strain and did not have the same failure process. In fact, although the random field was controlled using the same parameters, the arrangement of the thickness was quite different. In this case, the weakest single element or area in

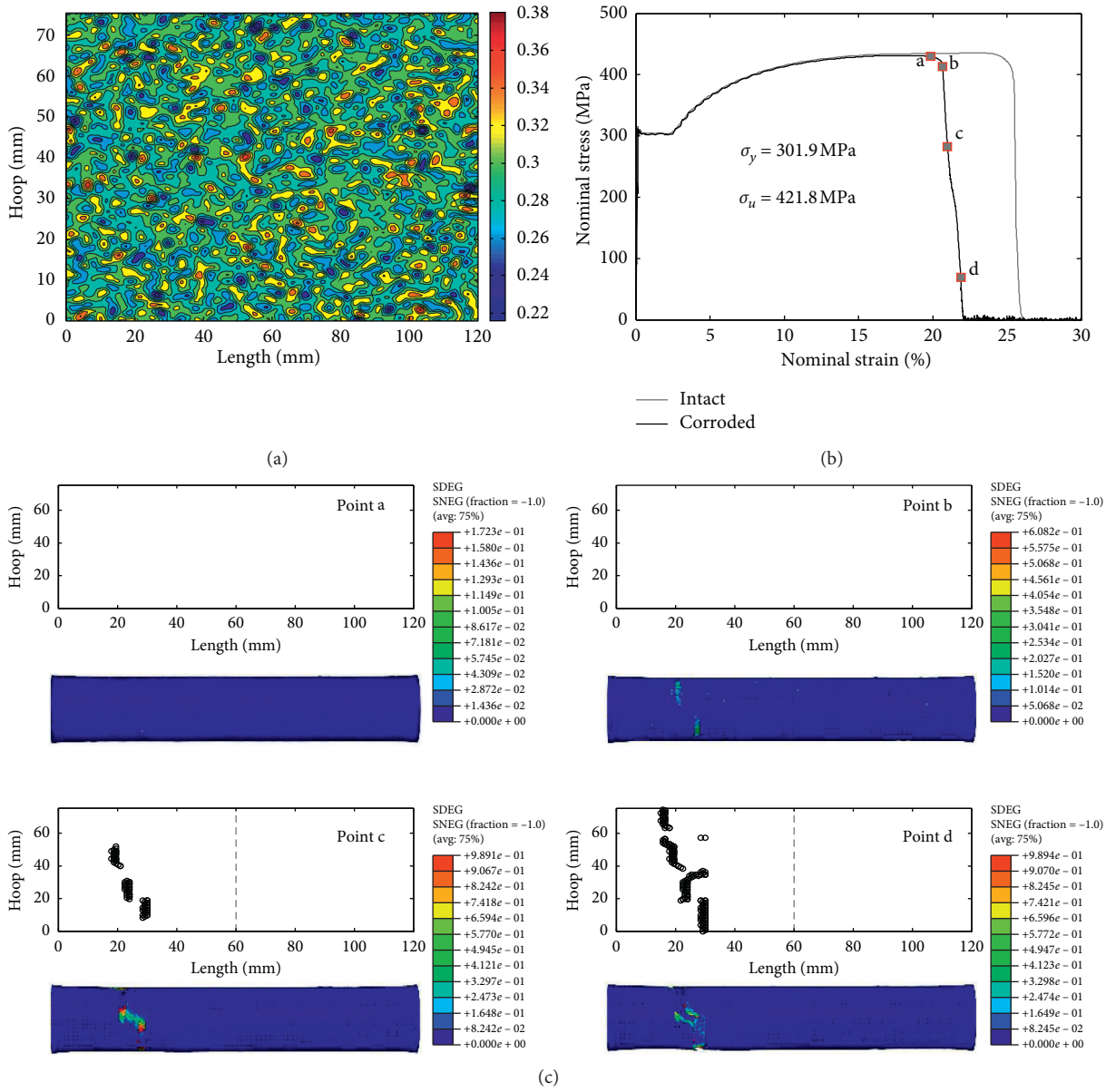


FIGURE 12: Damage evolution and fracture mode of a corroded pipe. (a) Random field with a value of $\eta$ = 70% and var = 0.02 mm, (b) stress-strain curve, and (c) crack propagation at points marked in (b).

the model frequently fractures first and then quickly expands into the surrounding regions. Therefore, this phenomenon makes it difficult for the specimen to exhibit the same failure mode under the same boundary and loading conditions.

*3.4. Influence of Variance.* To investigate the influence of the variance on the macroscopic properties of the corroded specimen, a comparison was performed on the simulation results with variables, $\eta$ = 70% and $\delta$ = 0.02 mm, as shown in Figure 12, and the results with variables $\eta$ = 70% and $\delta$ = 0.10 mm, as shown in Figure 10.

A careful comparison of these two series of figures shows that under the same corrosion rate, a difference in standard variance may lead to a markedly different strength, fracture strain, and fracture modes. This is because when the standard variance is small, the thickness difference of each element is slight. While the pipe model is stretched, there are more elements close together to resist the generation and development of cracks. Additionally, with an increase in standard variance, the difference in the thickness of the element also increases, and the thinner elements are inclined to fail under a relatively small stretching strain. Hence, only the remaining parts continue to resist the development of the crack, thereby causing a decrease in the strength and plastic deformation. This indicates that the standard variance of the distribution of different thickness elements has an essential influence on the mechanical properties and stability of the pipeline.

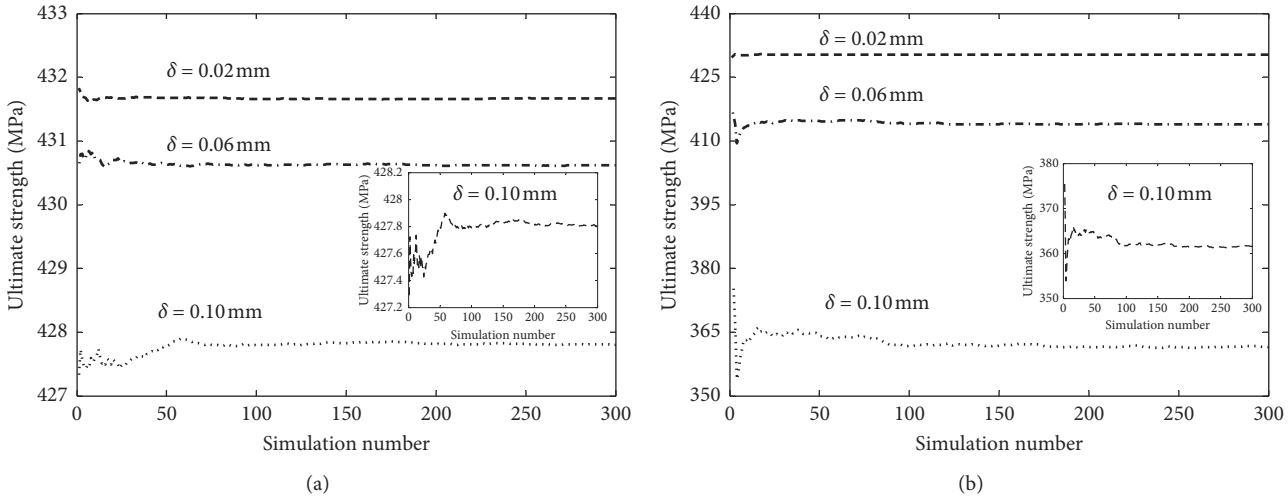


Figure 13: Effect of sample number on the mean value of ultimate tensile strength. (a) $\eta$ = 15% and (b) $\eta$ = 70%.

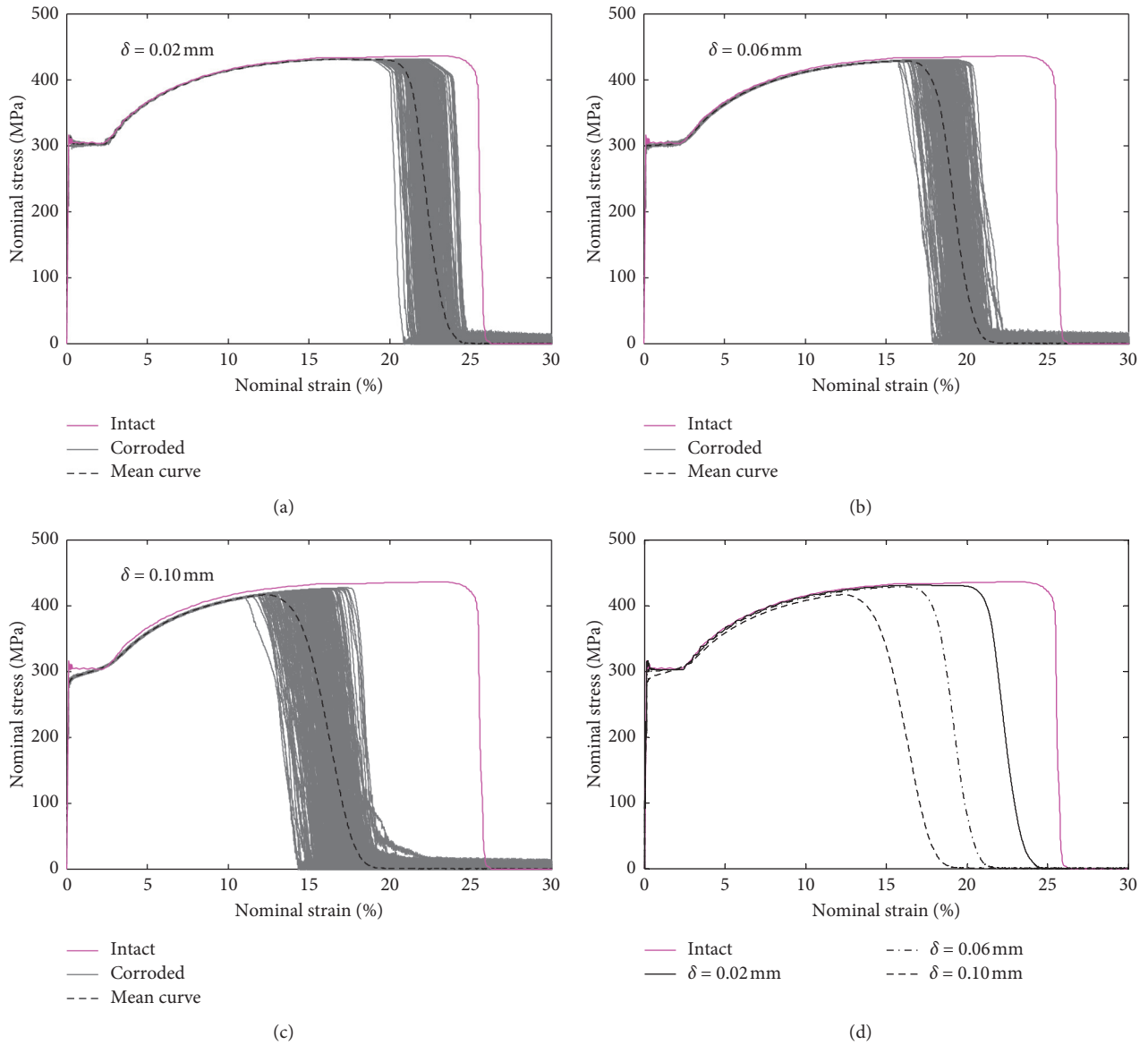


Figure 14: Stress-strain curves predicted using MCS with 300 samples ($\eta$ = 45%).

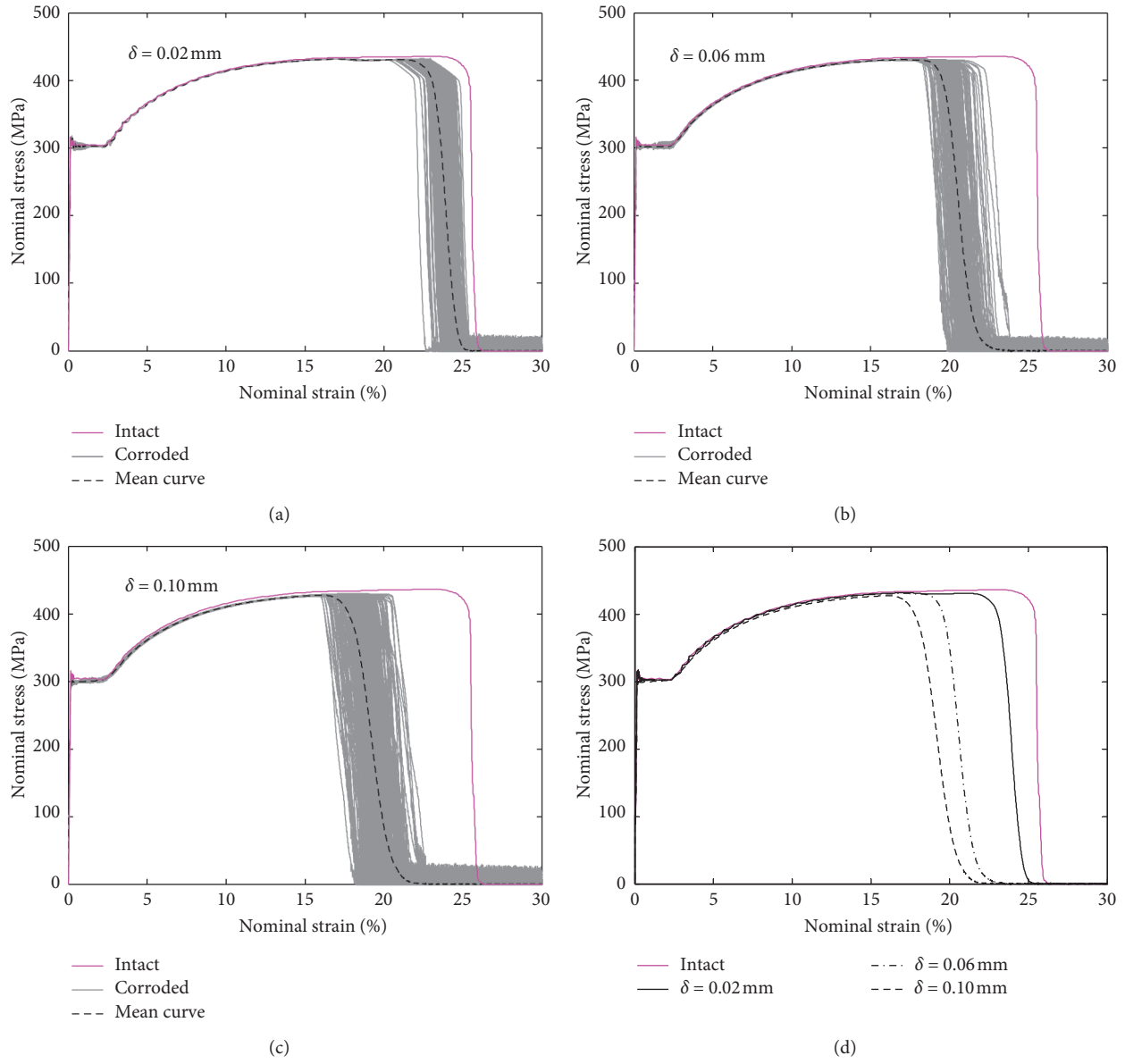


Figure 15: Stress-strain curves predicted using MCS with 300 samples ($\eta$ = 15%).

It should be noted that the use of the macroscopic stress in this work was established using $\sigma^{C} = F/A^{C}$ to evaluate the performance of the corroded specimen. Therefore, theoretically, the area reduction should not cause a reduction in the strength and plastic deformation. The degradation in the strength and change of failure modes are results of the unevenness of the thickness along the surface of the specimen.

## 4. Results Based on Monte Carlo Simulation

To explore the influence of the corrosion rate and standard variance on the thickness in the random distribution field, three series of pipelines with average wall thicknesses of 0.3 mm, 0.55 mm, and 0.85 mm, namely,$\eta$ = 70%, 45%, and 15%, and three variances, $\delta$ = 0.02, 0.06, and 0.10 mm, were considered in the generation of the random distribution. In one MCS, 300 random typology samples were generated. In total, 9 MCSs were conducted with 2,700 random samples generated, and the same number of nonlinear analyses was performed.

*4.1. The Influence of Simulation Number.* To guarantee the results reflected the trend of the corroded specimen in a stable manner, the mean value of stress in the previous $m$ simulations was defined as

$$\overline{\sigma} = \frac{1}{m}\sum_{i=1}^{m}\sigma_i\Big|_{m=1,300}. \quad (7)$$

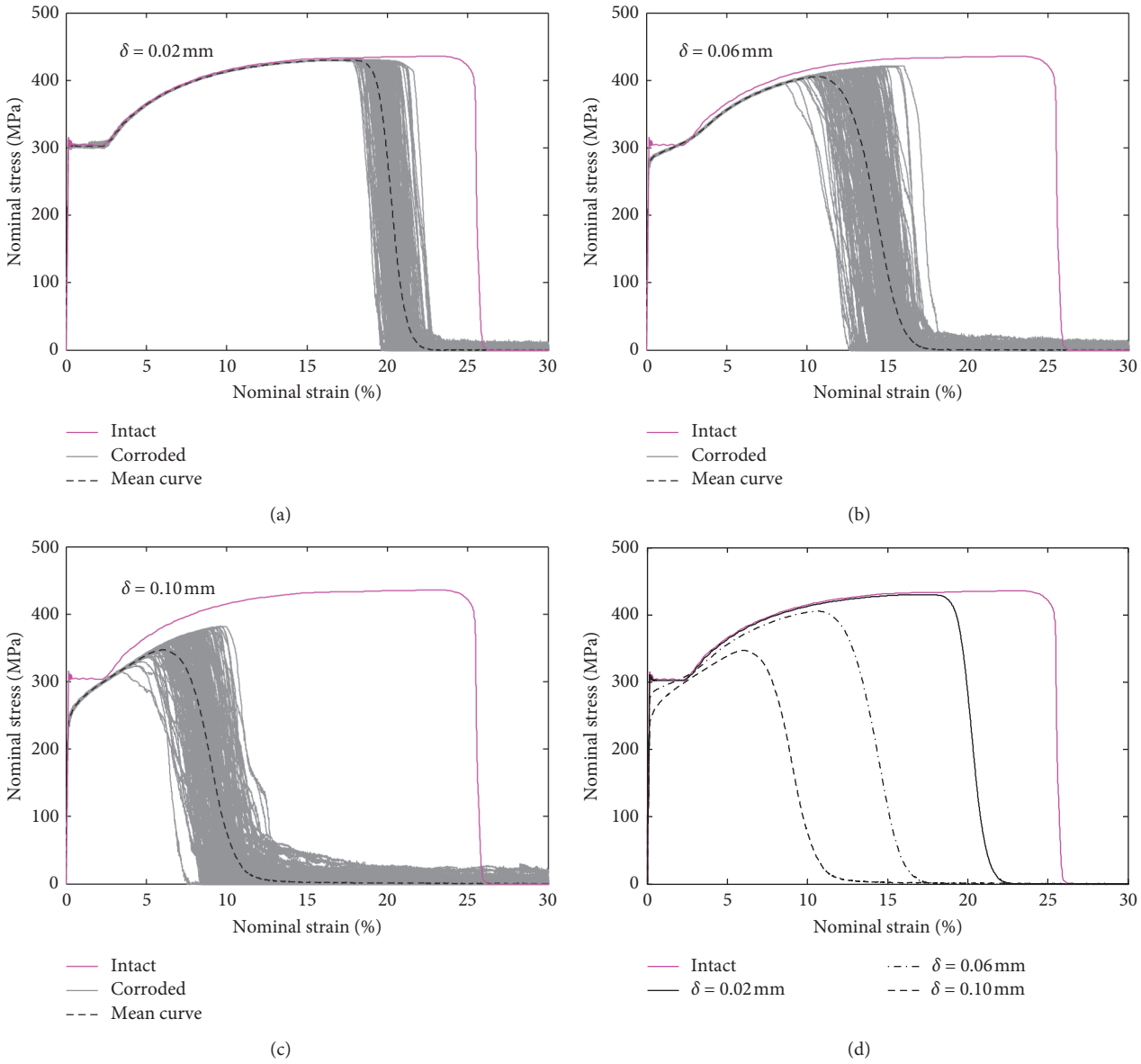


Figure 16: Stress-strain curves predicted using MCS with 300 samples ($\eta$ = 70%).

The average values of the stress for two corrosion rates and three standard variances as a function of number of the simulations are summarized in Figure 13. It can be seen that the mean value of the stress fluctuates significantly when the number used in the analysis is small and becomes stable when the number is bigger than 200. This phenomenon hints that, for the corroded specimen, the separated analysis may only reveal the variation of the degradation in the specimen in a qualitative way but cannot capture it in quantitative way.

*4.2. Results of Monte Carlo Simulation.* The results of the MCS method with a corrosion rate of $\eta$ = 45% and three variances are summarized in Figures 14(a)–14(c), and the mean stress-strain curves are calculated and compared in Figure 14(d). The random distribution of the results confirms the observation of the test data and the separate analysis of the simulation. The average ultimate strengths are 430.0 MPa, 427.2 MPa, and 416.2 MPa for the specimen with three variances, respectively. Clearly, the variance of the random field had a dominant effect on the yield and ultimate strength, as indicated by the mean stress-strain curve. The high variance of the random distribution yielded lower peak stress due to the uneven thickness distribution that covered the entire specimen.

The results for the corrosion rate $\eta$ = 15% and $\eta$ = 70% are shown in Figures 15 and 16, from which one can observe a similar trend as shown in Figure 14.

Comparatively, it is interesting to note that when the variance is the same and the corrosion rate is different, the yield stress and ultimate strength are quite different. This is

because even if the variance is the same, the higher the corrosion rate, the smaller the overall wall thickness of the element, and the lower the ability to resist crack generation and development. This implies that the corrosion rate also has an important influence on the performance of the pipe when the variance of the wall thickness distribution is the same. Therefore, the corrosion rate and variance will collaboratively affect the macroscopic properties of a corroded specimen.

From the viewpoint of the engineering, when the corrosion rate and variance of the aged pipelines are tremendous, the weakest section or crack path can be more easily detected as fewer weak elements contributed to fracturing resistance and then result in a lower peak strength. The present simulation indicates that a higher corrosion rate with high heterogeneity in the thickness always makes the pipeline have a lower yield and ultimate strength from the macroscopic view. In many structural design codes and research reports, the design strength of a corroded pipe is evaluated based on some specific defect shapes (e.g., [19, 22]), which is frequently obtained from the mechanical process. This may not truly reflect the real corroded surface caused by environmental erosion, nor can it be used to predict the degrading behavior of such components with high accuracy.

In addition, as an extension of the deterministic analysis method adopted in this series of paper, the probabilistic physical modelling method presented in [29, 30] has been proven to be a powerful tool for assessment of the lifetime risk of cast iron pipelines. It provides a new perspective to explore the long-term mechanical behavior and fragility of the pipeline in a statistical way and deserves further attention.

## 5. Conclusions

Inspired by the SEM photographs of the surface topology of the corroded specimen and the scatter distribution of the test results, a computational procedure was developed to simulate the randomness of the crack propagation process in a corroded specimen with random heterogeneous surface thicknesses. A total of 2,700 numerical pipeline models, which have three corrosion rates and three standard variances, were subjected to tensile tests. The following main conclusions can be drawn:

(1) The dispersion of wall thickness caused by environmental erosion will lead to stress concentration at the weak position of the pipeline and then induce the randomness of the crack propagation, which gives a reasonable explanation for the experimental failure mode of the corroded pipe.

(2) The corrosion rate and standard deviation of the wall thickness will jointly control the tensile behavior of the corroded pipe. When the corrosion rate is the same, the dispersion of the cross-section represented by the increase of the standard deviation is easy to generate stress concentration in the weak part and leads to the chain fracture phenomenon in the subsequent section. When the standard deviation is the same, the pipe with a higher corrosion rate is more likely to break at the weak part, resulting in a decrease in the macroscopic strength. This mechanism reasonably explains the performance degradation trend exhibited by tensile tests on 210 corroded pipes.

(3) Due to the discreteness of the wall distribution, a single simulation can only obtain a qualitative analysis of this problem and fail to quantify its performance trends. The Monte Carlo theory-based simulation method developed in this paper provides the possibility for this work.

It is worth noting that the cross-section changes caused by natural environmental erosion are very complicated. Despite that the experiment and simulation work is carried out on the wide range of corrosion rate, it is still in the scope of general corrosion, and the tensile behavior of the pipe under the condition of pitting corrosion also needs extensive research work. In addition, during the service of the pipeline, it may be under the combined stress state of tensile (or compression), bending, or internal (external) pressure. The mechanism of mechanical behavior affected by the environmental erosion needs to be paid attention to in future research.

## Data Availability

The data used to support the findings of this study are included within the article.

## Conflicts of Interest

The authors declare that they have no conflicts of interest.

## Acknowledgments

This study was supported by the National Science Foundation of China (grant nos. 11672165 and 51208289).

## References

[1] C. I. Ossai, "Predictive modelling of wellhead corrosion due to operating conditions: a field data approach," *ISRN Corrosion*, vol. 2012, pp. 1–8, 2012.

[2] G. Fekete and L. Varga, "The effect of the width to length ratios of corrosion defects on the burst pressures of transmission pipelines," *Engineering Failure Analysis*, vol. 21, pp. 21–30, 2012.

[3] A. K. Pilkey, S. B. Lambert, and A. Plumtree, "Stress corrosion cracking of X-60 line pipe steel in a carbonate-bicarbonate solution," *Corrosion*, vol. 51, no. 2, pp. 91–96, 1995.

[4] A. Cosham, P. Hopkins, and K. A. Macdonald, "Best practice for the assessment of defects in pipelines—Corrosion," *Engineering Failure Analysis*, vol. 14, no. 7, pp. 1245–1265, 2007.

[5] M. S. Chiodo and C. Ruggieri, "Failure assessments of corroded pipelines with axial defects using stress-based criteria: numerical studies and verification analyses," *International Journal of Pressure Vessels and Piping*, vol. 86, no. 2-3, pp. 164–176, 2009.

[6] B. Ma, J. Shuai, D. Liu, and K. Xu, "Assessment on failure pressure of high strength pipeline with corrosion defects," *Engineering Failure Analysis*, vol. 32, pp. 209–219, 2013.
[7] ASME, "Manual of determining the remaining strength of corroded pipelines," 1991.
[8] J. F. Kiefner and P. H. Vieth, "A modified criterion for evaluating the remaining strength of corroded pipe," *Materialsence*, vol. 10, 1989.
[9] DNV, "Recommend practice, RP-F101, corroded pipelines," *Det Norske Veritas*, vol. 25, 2000.
[10] Y. Bai and S. Hauch, "Collapse capacity of corroded pipes under combined pressure, longitudinal force and bending," *International Journal of Offshore and Polar Engineering*, vol. 11, no. 1, pp. 55–63, 2001.
[11] M. Zheng, J. H. Luo, X. W. Zhao, G. Zhou, and H. L. Li, "Modified expression for estimating the limit bending moment of local corroded pipeline," *International Journal of Pressure Vessels and Piping*, vol. 81, no. 9, pp. 725–729, 2004.
[12] L.-H. Han, S.-Y. He, Y.-P. Wang, and C.-D. Liu, "Limit moment of local wall thinning in pipe under bending," *International Journal of Pressure Vessels and Piping*, vol. 76, no. 8, pp. 539–542, 1999.
[13] Y.-J. Kim, C.-K. Oh, C.-Y. Park, and K. Hasegawa, "Net-section limit load approach for failure strength estimates of pipes with local wall thinning," *International Journal of Pressure Vessels and Piping*, vol. 83, no. 7, pp. 546–555, 2006.
[14] Y. Lei and P. J. Budden, "Limit load solutions for thin-walled cylinders with circumferential cracks under combined internal pressure, axial tension and bending," *The Journal of Strain Analysis for Engineering Design*, vol. 39, no. 6, pp. 673–683, 2004.
[15] S. Rahman and G. Wilkowski, "Net-section-collapse analysis of circumferentially cracked cylinders-part I: arbitrary-shaped cracks and generalized equations," *Engineering Fracture Mechanics*, vol. 61, no. 2, pp. 191–211, 1998.
[16] S. Rahman, "Net-section-collapse analysis of circumferentially cracked cylinders-part II: idealized cracks and closed-form solutions," *Engineering Fracture Mechanics*, vol. 61, no. 2, pp. 213–230, 1998.
[17] Y. C. Yang, F. Liu, and F. Xi, "Tensile fracture behavior of corroded pipeline, Part 1: experimental characterization," *Advances in Materials Science & Engineering*, vol. 2020, Article ID 4058452, 14 pages, 2020.
[18] J. A. Filho, R. D. Machado, R. J. Bertin et al., "On the failure pressure of pipelines containing wall reduction and isolated pit corrosion defects," *Computers and Structures*, vol. 132, pp. 22–33, 2014.
[19] Y. Shuai, J. Shuai, and K. Xu, "Probabilistic analysis of corroded pipelines based on a new failure pressure model," *Engineering Failure Analysis*, vol. 81, pp. 216–233, 2017.
[20] A. Kolios, S. Srikanth, and K. Salonitis, "Numerical simulation of material strength deterioration due to pitting corrosion," *Procedia CIRP*, vol. 13, pp. 230–236, 2014.
[21] T. A. Netto, U. S. Ferraz, and S. F. Estefen, "The effect of corrosion defects on the burst pressure of pipelines," *Journal of Constructional Steel Research*, vol. 61, no. 8, pp. 1185–1204, 2005.
[22] G. H. Lee, H. Pouraria, J. K. Seo, and J. K. Paik, "Burst strength behaviour of an aging subsea gas pipeline elbow in different external and internal corrosion-damaged positions," *International Journal of Naval Architecture and Ocean Engineering*, vol. 7, no. 3, pp. 435–451, 2015.
[23] Simulia, "Abaqus analysis user's manual," 2013.
[24] M. Shinozuka and C.-M. Jan, "Digital simulation of random processes and its applications," *Journal of Sound and Vibration*, vol. 25, no. 1, pp. 111–128, 1972.
[25] X. F. Xu and L. Graham-Brady, "A stochastic computational method for evaluation of global and local behavior of random elastic media," *Computer Methods in Applied Mechanics and Engineering*, vol. 194, no. 42–44, pp. 4362–4385, 2005.
[26] MATLAB, https://www.mathworks.com/.
[27] M. S. Mirza, D. C. Barton, and P. Church, "The effect of stress triaxiality and strain-rate on the fracture characteristics of ductile metals," *Journal of Materials Science*, vol. 31, no. 2, pp. 453–461, 1996.
[28] T. Wierzbicki, Y. Bao, Y. W. Lee et al., "Calibration and evaluation of seven fracture models," *International Journal of Mechanical Sciences*, vol. 47, no. 4-5, pp. 719–743, 2005.
[29] J. Ji, D. J. Robert, C. Zhang, D. Zhang, and J. Kodikara, "Probabilistic physical modelling of corroded cast iron pipes for lifetime prediction," *Structural Safety*, vol. 64, pp. 62–75, 2017.
[30] J. Ji, J. H. Lai, G. Y. Fu et al., "Probabilistic failure investigation of small diameter cast iron pipelines for water distribution," *Engineering Failure Analysis*, vol. 108, pp. 1–14, 2020.